ONLINE RESOURCE

1. Neuroimaging Acquisition & Processing Procedures

Neuroimaging data was acquired as part of an AVID Radiopharmaceuticals sponsored clinical trial.

PET Methods. PET scans were acquired using a Philips Ingenuity TF PET/CT scanner at the PET Center in the Department of Radiology of the University of Pennsylvania. In one session ^{18}F-florbetapir was administered and confirmed visually negative for amyloid-positivity by AVID Radiopharmaceuticals. In two separate sessions (15 months and 5 months prior to death) ^{18}F-AV-1451 (formerly ^{18}F-T807) was administered intravenously to the patient who was then scanned 75-105 minutes after injection of a target ^{18}F-AV-1451 dose of 370MBq (10 mCi). For ^{18}F-AV-1451 whole brain PET volumes were acquired in 6 5-minute frames at a 2mm^3 resolution in a 128 x 128 x 90 voxel matrix. PET data were corrected for signal attenuation and patient head motion, then summed across the 6 acquisition frames. A rigid-body alignment was computed to register native-space PET images to each patient's accompanying T1 image. In an effort to account for grey matter atrophy we performed partial volume correction using the Structural-Functional Synergistic Resolution Recovery (SFS-RR) method[13]. Briefly, this method replaces high spatial frequencies in a static PET image with the corresponding frequencies in a high-resolution structural brain image, with supervision from a probabilistic brain atlas and appropriate scaling to adjust for differences in signal magnitude between PET and structural imaging data.

PET volumes were then normalized to a reference region defined by warping a cerebellum atlas [4] from Montreal Neurological Institute (MNI) space to each patient's native PET acquisition space. The ^{18}F-AV-1451 signal was averaged over all cerebellar grey matter, except for the deep grey nuclei, to establish a patient-specific uptake reference value. Our neuropathological evaluation assessed cerebellum dentate nucleus grey matter and it revealed minimal tau pathology (%AO=0.5) and qualitatively the remainder of the cerebellum only had rare pathology. Therefore given the minimal pathological burden we felt this region was

OK to use for our reference. Every voxel in the motion-corrected, summed PET volumes were divided by the cerebellar reference value to create a specific uptake value ratio (SUVR) map for each patient. SUVR maps were spatially aligned with each patient's accompanying T1 image and the template image and smoothed with an 8 mm Gaussian kernel. We then derived regional SUVR measures using a series of well-annotated atlases including 100 cortical[6], 34 deep grey[10], and 48 white matter[11] labels.

MRI Methods. High resolution T1-weighted MPRAGE MRI volumes were acquired from a SIEMENS 3.0T Trio scanner with an 8-channel coil (repetition time=1620msec; echo time=3msec; slice thickness=1.0mm; flip angle=15°; matrix=192×256, and in-plane resolution=0.9×0.9mm). Diffusion-weighted images were acquired with either a 30-directional or 12-directional acquisition sequence. The 30-directional sequence included a single-shot, spin-echo, diffusion-weighted echo planar imaging sequence (FOV=240mm; matrix size=128×128; number of slices=70; voxel size=2mm isotropic; TR=8100ms; TE=83ms; fat saturation). In total, 35 volumes were acquired per subject, five without (b=0s/mm2) and 30 with diffusion weighting (b=1000s/mm2) along 30 non-collinear directions. The 12-directional sequence included a single-shot, spin-echo, diffusion-weighted echo planar imaging sequence (matrix size=128×128, number of slices=40, voxel size=1.7x1.7x3mm; TR=6500ms, TE=99ms). In total 12 non-collinear, non-coplanar, isotropic diffusion encoding directions were acquired.

All image preprocessing was performed using Advanced Normalization Tools (ANTs) which provides a state-of-the-art pipeline [16]. Briefly, this pipeline includes N4 bias correction to minimize image inhomogeneity effects [15], brain extraction, and Atropos six-tissue class segmentation (cortex, deep grey, brainstem, cerebellum, white matter, and CSF/other)[2]. We then generate voxelwise grey matter density measures, as previously reported [8] as the weighted probability of a voxel belonging to a given tissue class and use a diffeomorphic and symmetric registration algorithm to warp each GM density map to a custom template, The Penn

Neurodegenerative Disease Template, comprised of a representative neurodegenerative disease patients and aging controls.

Diffusion weighted (DW) images were preprocessed using ANTs software to generate mean diffusivity measurements. Briefly, the unweighted (b=0) images are first extracted and averaged. All DW images (including the individual b=0 volumes) are then aligned to the average b=0 using ANTs. An affine transform is applied to capture eddy distortion in the DW images as well as motion. Diffusion tensors are computed using a weighted linear least squares algorithm in Camino [3]. The corrected average b=0 image is aligned to the subject's T1 image from the same scanning session, first rigidly to correct for motion, then using a deformable diffeomorphic transformation with mutual information to correct for inter-modality distortion. The diffusion to T1 warp is composed with the T1 to template warp (from the cortical thickness pipeline), producing a mapping from DWI space to the population T1 template in a single interpolation. Tensors are resampled into the template space using log-Euclidean interpolation and reoriented to preserve the anatomical alignment of WM tracts [1].

To compare MRI and DTI results to SUVR uptake we used a multi-atlas label fusion technique [17] to evaluate adjusted grey matter volume (ROI_{volume} / Intracranial volume) in 100 cortical[6] and 34 deep grey[10] structures along with mean diffusivity in 44 cerebrum white matter[11] parcellations.

2. Clinical & Neuropsychological Details

We evaluated a male patient who suffered 2 falls, and subsequently developed dry eyes, difficulty focusing his vision, reduced facial expression, soft voice, and "mental fogginess." Previous medical history included hyperlipidemia, gastric reflux, and untreated mild obstructive sleep apnea. He was first evaluated at 56 years of age and 3.5 years prior to death by a neuro-ophthalmologist, at which time his neuro-ophthalmologic and neurologic exams were unrevealing. Subsequent evaluation by an outside neurologist led to a diagnosis of Parkinson's disease and initiation of selegiline followed by carbidopa-levodopa with a good response.

At the time of initial movement disorders specialist evaluation, 2.5 years prior to death, he complained of difficulty tracking across a page while reading, his spouse reported mildly inappropriate behavior with disinhibition, and the carbidopa-levodopa effect had waned, with side effects of nausea and dizziness. Neurologic exam revealed limited downgaze, severely impaired vertical saccades, absent downward optokinetic reflex, preserved vestibulo-ocular reflex, mild to moderate asymmetric left-sided limb rigidity, and a mild gait disorder involving reduced left arm swing without postural instability. Trials of various dopaminergic agents and antidepressants provided no relief. At this time the patient received a diagnosis of progressive supranuclear palsy (PSP) and this clinical diagnosis was sustained for the remainder of the patient's life.

Two years prior to death, he began experiencing more postural unsteadiness with additional falls. He had worsening motor slowing and stiffness that was more prominent on the left. One and one-half years prior to death and at 58 years old, near the time of his baseline MRI and ^{18}F-AV-1451 scan, the patient experienced more rapid motor decline, involving ophthalmoparesis, eyelid-opening apraxia, dysphagia, relentlessly progressive immobility, severe axial rigidity, and postural instability with spontaneous retropulsion. He also developed impulsive behaviors with poor judgment, such as opening a car door while in motion.

MoCA screening two years prior to death revealed a score of 21/30, with points lost for reverse digit and sentence repetition, attention, phonemic category naming fluency and delayed recall. A more detailed neuropsychological evaluation was performed at the time of the patient's first ^{18}F-AV-1451 scan that was 15 months prior to his death (see Table below). At this time his MoCA score was 23/30 consistent with mild impairment. He exhibited severe deficits with processing speed on Trail-Making Test Part A and mental flexibility on Trail-Making Test Part B, and moderate deficits on category letter fluency (Z-score -2.35).

Here we provide a summary of the patient's neuropsychological performance at the time of the baseline ^{18}F-AV-1451 scan:

Domain	Tests	Score	Z-score	Description
Global	**Global Screen:** Mini-Mental State Examination (MMSE) (30 points) Montreal Cognitive Assessment (MoCA) (30 points)	29 23	-0.03 -2.00	Average Mildly Impaired
Language/Semantic	**Semantic Fluency**: Generation of animals in 1 minute	15	-1.37	Mildly Impaired
Memory	**Verbal Memory:** Rey Auditory Verbal Learning Test (RAVLT; 15 words) • Total recall after 5 learning trials • Immediate recall • Delayed recall • Yes-no recognition trial: P(A)	35 7 5 0.9	-1.50 -0.71 -1.23 0	Mildly Impaired Low average Low Average Average
Visuospatial / Constructional	**Visuospatial Abilities:** Visual Object and Space Perception Battery (VOSP) • Object Decision (20 items)	15	-1.42	Mildly Impaired
Attention / Working Memory	Forward Digit Span Backward Digit Span	6 3	-0.87 -1.80	Low Average Mildly Impaired
Processing Speed	Trail-Making Test A (TMT-A) (time to completion). 23/24 correct lines	85"	-4.23	Severely Impaired
Executive Function	**Verbal generation:** Category Letter Fluency (words starting with "F", "A" and "S" in 1 minute – total score) **Mental Flexibility:** Trail-Making Test B (TMT-B) (serial alternation between numbers and letters-time to completion). 21/24 correct lines	16 181"	-2.35 -2.67	Moderately Impaired Severely Impaired

3. Annualized change in ^{18}F-AV-1451 retention.

Figure. Relationships between annualized change in ^{18}F-AV-1451 retention. Associations of ^{18}F-AV-1451 retention with (left) baseline MRI grey matter volume, (middle) baseline mean diffusivity, and (right) AT-8 area occupied of post-mortem tau.

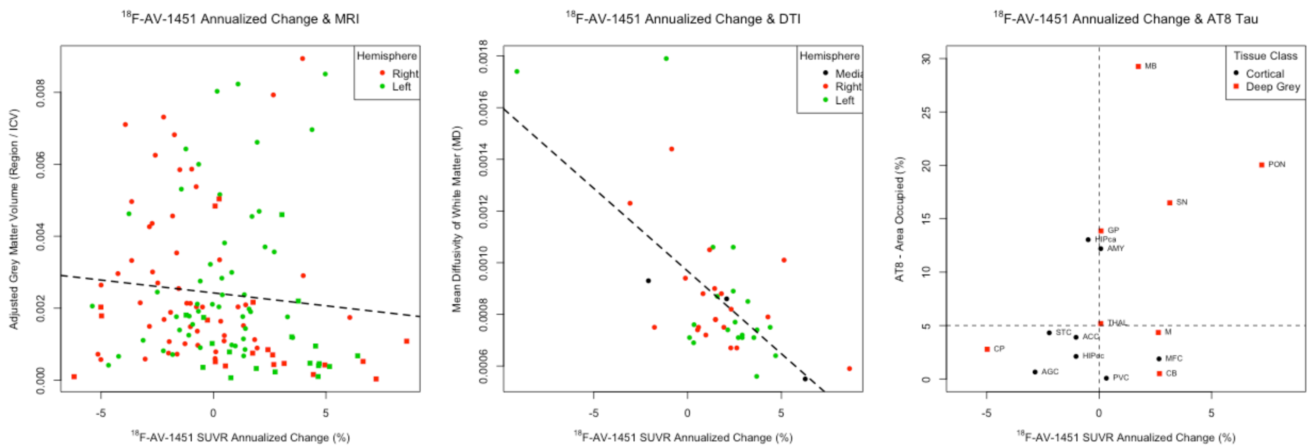

4. Gross Neuropathological Examination & Immunohistochemistry

All neuropathological assessments were performed using a previously described procedure[14], by an expert neuropathologist (JQT) who was blinded to the patient's clinical history and imaging results.

Gross Examination. The brain was examined 3 hours postmortem and it weighed 1,262 grams. Both external and internal surfaces of the dural leaflets were smooth and free from nodules. The superior sagittal sinus was patent. The external surfaces of the brain were symmetric and exhibited mild frontal pole atrophy without softening or discoloration. There was no evidence of herniation of the cingulate gyri, uncus or cerebellar tonsils. The leptomeninges were thin translucent and free from exudate. Examination of the arteries of the Circle of Willis and their major branches revealed that they were patent, with mild atherosclerosis. The superficial veins of the brain were unremarkable. Serial coronal sections revealed unremarkable cortex and centrum ovale. The cerebral cortex had an average thickness of 4-5 mm. The ventricles were symmetrical and without dilatation. There was no deviation of the septum pellucidum. There was no evidence of infarction, hemorrhage, or tumor mass. The nuclei of the brain, including the thalami, the caudate, the lentiform, the lateral geniculate bodies and the subthalamic nuclei were unremarkable. The hippocampus and amygdala were unremarkable. The substantia nigra was moderately depigmented and the locus coeruleus was mildly depigmented. The internal capsules, the cerebral peduncles, the pons, the medulla, the cerebellar hemispheres, the vermis and the cerebellar nuclei were all unremarkable. Portions of the right hemisphere were frozen and left hemisphere regions were fixed in ethanol and neutral buffered formalin for microscopic examination using immunohistochemistry (IHC).

Immunohistochemistry (IHC). We performed IHC for detecting tau, β-amyloid, TDP-43, and alpha-synuclein. Tau-directed IHC included monoclonal antibodies directed at phosphorylated tau [PHF-1, mAb, 1:1000, a gift from Dr. Peter Davies; AT-8, Thermo Scientific, Waltham, MA[9]) and 3- and 4-repeat tau isoforms (RD3, RD4), Millipore, Billerica, MA, USA]. Regions sampled (N=16) for IHC include the anterior cingulate cortex (ACC), middle frontal cortex (MFC), superior temporal cortex, angular cortex, visual cortex, amygdala, hippocampus CA1/subiculum, entorhinal cortex, thalamus, substantia nigra, putamen, lentiform nucleus (globus pallidus), midbrain, medulla, pons, and cerebellum (dentate nucleus).

We confirmed 4R tauopathy using tau-isoform specific antibodies and found the tau pathology to be exclusively 4Rtau positive with the exception of rare (1-2 total) 3Rtau tangles in peri-amygdalar cortex and entorhinal cortex that we interpret as age related rather than CBD related. Western blot analyses using a preparation of detergent-insoluble fraction obtained from frozen putamen and temporal cortex[7, 18] further confirmed the presence of pathological tau composed of 4R and not 3R isoforms, which is typical of CBD and very distinct from AD and Pick's disease as illustrated in the figure below and previously reported[5, 12]. Representative examples of tau inclusions are reported in the following figure:

Figure. Neuropathological & Biochemistry findings. Photomicrographs depict CBD tauopathy found at autopsy (scale bar=100 um). a) Substantia nigra with severe burden of neuritic threads and phosphorylated tau-positive inclusions in remaining pigmented neurons (arrow). b) Lentiform with high burden of tau-reactive threads, tangles and coiled bodies (arrows) in white matter oligodendrocytes. c) Superior temporal cortex grey matter with numerous superficial cortical layer tau tangles (arrows) and diffuse threads (asterisks) and d) temporal white matter with mild-to moderate tau-positive axonal threads (asterisks). e) Mid-frontal cortex contained frequent astrocytic plaques (asterisk) and f) mild to moderate axonal threads (asterisks) and tau-reactive coiled bodies (arrow) in adjacent frontal white matter. g) Glial and neuronal (arrow) tau pathology was reactive to 4R tau isoform specific antibody but h) not reactive for 3R tau (superior temporal cortex). SDS-PAGE Western blotting of Triton X-100-insoluble fraction extracted from fresh frozen brain tissue (i-l) with immunolabeled banding patterns of total-tau (17025; i), phosphorylated-tau (PHF-1; j) and 4R tau isoforms (RD4; k) consistent with 4R tauopathy and absence of 3R tau isoforms (RD3; l) as is typical of CBD. TC = temporal cortex (patient sample), Put = putamen (patient sample); AD, CBD, and PiD = Pick's disease, as control samples are also shown.

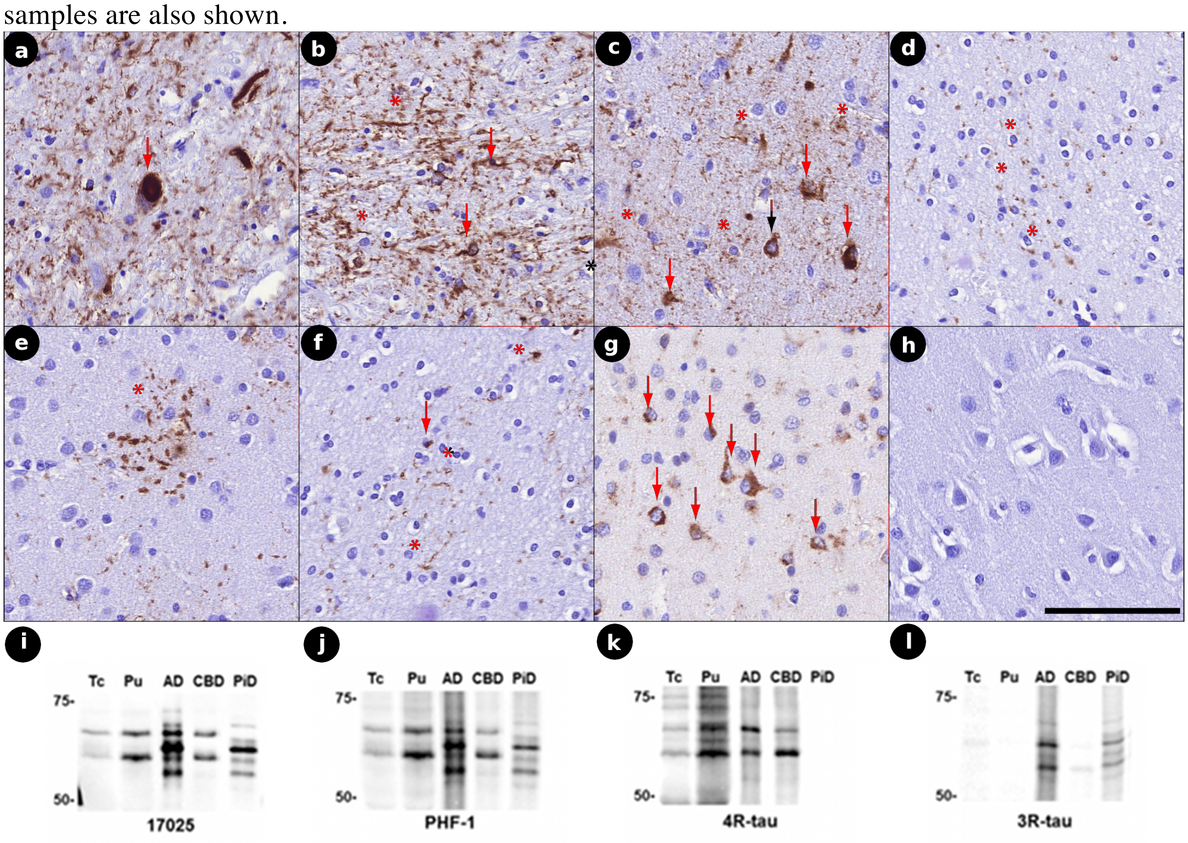

All other IHC revealed no additional forms of neurodegenerative inclusions such as deposits of Aβ amyloid, TDP-43 or alpha-synuclein Lewy bodies or neurites as well as no other lesions including vascular pathology or hippocampal sclerosis. A lack of Aβ amyloid pathological burden is consistent with the Aβ amyloid-negative ^{18}F-florbetapir PET scan from this patient.

5. Association of Neuroimaging Atrophy with Pathology-Defined SUVR.

Grey matter MRI and white matter diffusion tensor imaging (DTI) correlations with baseline ^{18}F-AV-1451 SUVRs (manuscript Figure 2) revealed significantly inverse associations with "raw" neuroimaging values. While grey matter volume adjusted for intracranial volume and mean diffusivity are generally considered reliable measures of atrophic brain, one could argue that interpretation of these values requires a comparison to normative data in order to define which regions are "atrophic". Therefore we calculated a Z-score for each region of interest (ROI) relative to a cohort of 100 demographically-comparable healthy controls who self-reported no history of neurological or psychiatric impairment. Since our evaluation of pathological tau and ^{18}F-AV-1451 suggested that a SUVR>1.2 captured all ROIs with high tau pathology (>5%) and did not capture any ROIs with low tau pathology (<5%), we then assessed the distribution of grey matter and white matter Z-scores using this pathologically-defined cutoff of SUVR>1.2. This revealed that Z-scores reflecting the magnitude of atrophy relative to controls were significantly lower for ROIs with higher SUVRs than lower SUVRs in deep grey matter (W=240, p=0.027) and white matter (W=307, p=0.052). We did not observe more atrophy for cortical grey matter ROIs with a SUVR>1.2 (W=205, p=0.826), though there were only 4 cortical ROIs that achieved a SUVR>1.2 and therefore difficulty to reliably assess. Notably, for white matter nearly every region with an SUVR>1.2 was identified as being atrophic (Z-score <0).

Figure. Associations Between Pathology-Defined SUVR Cutoff & Neuroimaging Measures of Brain Atrophy. Each plot illustrates the distribution of Z-scores for each evaluated region of interest (ROI) within those ROIs with baseline ^{18}F-AV-1451 SUVR < 1.2 (red) and ^{18}F-AV-1451 SUVR > 1.2 (blue): (left) cortical grey matter ROIs, (center) deep grey matter ROIs, and (right) white matter ROIs.

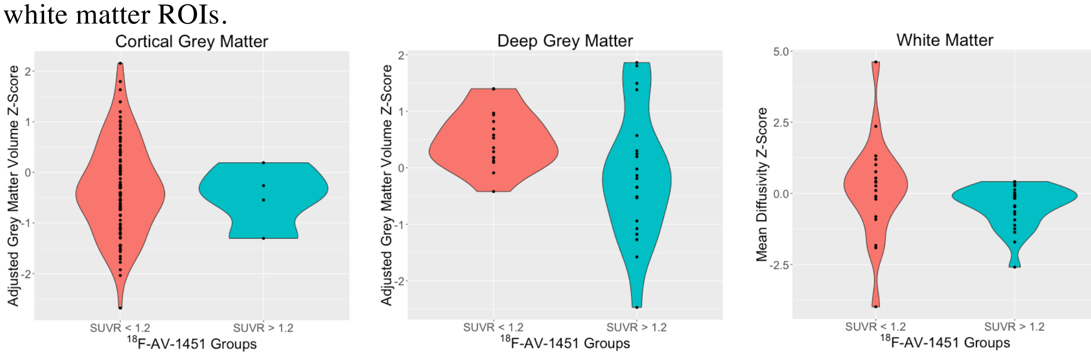

Online References

1. Arsigny V, Fillard P, Pennec X, Ayache N (2006) Log-Euclidean metrics for fast and simple calculus on diffusion tensors. Magn Reson Med 56:411–421.

2. Avants BB, Tustison NJ, Wu J, Cook PA, Gee JC (2011) An open source multivariate framework for n-tissue segmentation with evaluation on public data. Neuroinformatics 9:381–400.

3. Cook P, Bai Y, Nedjati-Gilani S (2006) Camino: Open-source diffusion-MRI reconstruction and processing. International Society for Magnetic Resonance Imaging in Medicine 2759.

4. Diedrichsen J, Balsters JH, Flavell J, Cussans E, Ramnani N (2009) A probabilistic MR atlas of the human cerebellum. NeuroImage 46:39–46.

5. Forman MS, Zhukareva V, Bergeron C, Chin SS-M, Grossman M, Clark C, et al. (2002) Signature tau neuropathology in gray and white matter of corticobasal degeneration. Am J Pathol 160:2045–2053.

6. Klein A, Tourville J (2012) 101 labeled brain images and a consistent human cortical labeling protocol. Front Neurosci 6:171.

7. Lowe VJ, Curran G, Fang P, Liesinger AM, Josephs KA, Parisi JE, et al. (2016) An autoradiographic evaluation of AV-1451 Tau PET in dementia. Acta Neuropathol Commun 1–19. doi: 10.1186/s40478-016-0315-6

8. McMillan CT, Wolk DA (2016) Presence of Cerebral Amyloid Modulates Phenotype and Pattern of Neurodegeneration in Early Parkinson's Disease. Journal of Neurology, Neurosurgery, and Psychiatry 87:1112-1122.

9. Mercken M, Vandermeeren M, Lübke U, Six J, Boons J, Van de Voorde A, et al. (1992) Monoclonal antibodies with selective specificity for Alzheimer Tau are directed against phosphatase-sensitive epitopes. Acta Neuropathol 84:265–272.

10. Oishi K, Faria A, Jiang H, Li X, Akhter K, Zhang J, et al. (2009) Atlas-based whole brain white matter analysis using large deformation diffeomorphic metric mapping: application to normal elderly and Alzheimer's disease participants. NeuroImage 46:486–499.

11. Oishi K, Zilles K, Amunts K, Faria A, Jiang H, Li X, et al. (2008) Human brain white matter atlas: identification and assignment of common anatomical structures in superficial white matter. NeuroImage 43:447–457.

12. Sander K, Lashley T, Gami P, Gendron T, Lythgoe MF, Rohrer JD, et al. (in press) Characterization of tau positron emission tomography tracer [(18)F]AV-1451 binding to postmortem tissue in Alzheimer's disease, primary tauopathies, and other dementias. Alzheimers Dement. doi: 10.1016/j.jalz.2016.01.003

13. Shidahara M, Tsoumpas C, Hammers A, Boussion N, Visvikis D, Suhara T, et al. (2009) Functional and structural synergy for resolution recovery and partial volume correction in brain PET. NeuroImage 44:340–348.

14. Toledo JB, Van Deerlin VM, Lee EB, Suh E, Baek Y, Robinson JL, et al. (2014) A platform for discovery: The University of Pennsylvania Integrated Neurodegenerative Disease Biobank. Alzheimers Dement 10:477–84.e1.

15. Tustison NJ, Avants BB, Cook PA, Zheng Y, Egan A, Yushkevich PA, et al. (2010) N4ITK: improved N3 bias correction. IEEE Trans Med Imaging 29:1310–1320.

16. Tustison NJ, Cook PA, Klein A, Song G, Das SR, Duda JT, et al. (2014) Large-scale evaluation of ANTs and FreeSurfer cortical thickness measurements. NeuroImage 99:166–179.

17. Wang H, Yushkevich PA (2013) Multi-atlas segmentation with joint label fusion and corrective learning-an open source implementation. Front Neuroinform 7:27.

18. Zhukareva V, Mann D, Pickering-Brown S, Uryu K, Shuck T, Shah K, et al. (2002) Sporadic Pick's disease: a tauopathy characterized by a spectrum of pathological tau isoforms in gray and white matter. Ann Neurol 51:730–739.